

A marked correlation function analysis of halo formation times in the Millennium Simulation

Geraint Harker,^{*} Shaun Cole, John Helly, Carlos Frenk and Adrian Jenkins

Department of Physics, University of Durham, Science Laboratories, South Road, Durham DH1 3LE

7 June 2018

ABSTRACT

We study the environmental dependence of the formation epoch of dark matter haloes in the Millennium Simulation: a ten billion particle N -body simulation of standard Λ CDM cosmology. A sensitive test of this dependence – the marked correlation function – reveals highly significant evidence that haloes of a given mass form earlier in denser regions. We define a marked cross-correlation function, which helps quantify how this effect depends upon the choice of the halo population used to define the environment. The mean halo formation redshift as a function of the local overdensity in dark matter is also well determined, and we see an especially clear dependence for galaxy-sized haloes. This contradicts one of the basic predictions of the excursion set model of structure formation, even though we see that this theory predicts other features of the distribution of halo formation epochs rather well. It also invalidates an assumption usually employed in the popular halo, or HOD, models of galaxy clustering, namely that the distribution of halo properties is a function of halo mass but not of halo environment.

Key words: cosmology: theory – dark matter – galaxies: haloes – galaxies: formation

1 INTRODUCTION

In the Cold Dark Matter paradigm, the large-scale structure of the Universe results from the amplification and evolution under gravity of small initial perturbations in the density distribution of massive, collisionless particles. On smaller scales, the clustering becomes nonlinear, and the dark matter collapses into relatively dense, virialized clumps – dark matter haloes. Gas falls into the potential wells created by these haloes, where it can cool and form stars (White & Rees 1978). It then seems as though the problem of understanding the properties and clustering of galaxies splits naturally into two parts – understanding the distribution of the haloes, and understanding the processes involving the dark matter and the baryonic components inside the haloes. This is clearly simplified if the two parts of the problem can be considered independently.

In current semi-analytic models of galaxy formation, the evolution of galaxies in haloes is driven by the merger histories of those haloes (e.g., Kauffmann, White & Guiderdoni 1993; Cole et al. 1994; Somerville & Primack 1999; Cole et al. 2000). We expect to be able to treat haloes independently of the large-scale structure if their merger histories are independent of the large-scale environment. This is also the basis of the halo occupation distribution (HOD) formalism (Seljak 2000; Berlind & Weinberg 2002; Cooray & Sheth 2002). Support for making this simplification has come from extended Press-Schechter theory (Bond et al. 1991; Bower 1991; Lacey & Cole 1993), which predicts that the

distribution of halo formation times is a function of halo mass but not of halo environment. This theory is the basis for the construction of Monte Carlo merger trees for semi-analytic models. To reach this conclusion, however, three simplifying assumptions are made, which if relaxed may result in an environmental dependence. Firstly, in order to solve the cloud-in-cloud problem (Bardeen et al. 1986) it is assumed that the trajectories, $\delta(M)$, in overdensity versus mass scale can be treated as Brownian random walks. This is only true when the density field is filtered with a sharp k -space filter. For a more natural top-hat or Gaussian filter the $\delta(M)$ trajectories exhibit correlations between different mass scales, which induce correlations between environment and small scale behaviour (Bond et al. 1991; Lacey & Cole 1993). Secondly, the extended Press-Schechter or excursion set theory deals only with individual mass points in the density field. When it predicts that a mass point is part of a halo of mass M there is no constraint that the whole of a neighbouring volume of mass M is also assigned to the same halo. The accuracy to which this assumption holds may depend on environment. Thirdly, in determining when a region collapses to form a halo, a global collapse threshold given by the spherical collapse model is assumed. It has been argued that tidal fields modify this threshold (Sheth, Mo & Tormen 2001) and these could also depend on environment.

Thus there is no compelling reason to believe that the lack of environmental dependence predicted by the Press-Schechter theory should carry over to a full treatment which relaxes these assumptions. It has been supported by N -body calculations, however, e.g. by Lemson & Kauffmann (1999) who used the GIF simulations

^{*} E-mail: g.j.a.harker@durham.ac.uk

(Jenkins et al. 1998; Kauffmann et al. 1999). Provided such simulations have sufficiently many outputs at different times, merger trees can be extracted and their environmental dependence studied. This approach has been limited by the dynamic range of the available simulations. Either galaxy-sized haloes have not been well resolved, leaving their merger histories uncertain, or the volume has not been cosmologically representative.

Galaxy properties, however, do depend on environment. Galaxies in denser regions tend, for example, to be more bulge-dominated and to have older stellar populations (e.g., Dressler 1980; Postman & Geller 1984; Gómez et al. 2003; Balogh et al. 2004). In models in which the merger histories of haloes are only a function of halo mass, and in the absence of non-local gas processes (e.g. ionization by QSOs), this can only be accounted for by the variation of the halo mass function with environment, or, in other words, by the fact that high mass haloes are more clustered than low mass haloes (Cole & Kaiser 1989; Mo, Mao & White 1999). Models which attempt to reproduce environmental dependence can then do so only by populating more massive haloes with a greater fraction of early-type galaxies.

None the less, Sheth & Tormen (2004) argue that one of the results of Lemson & Kauffmann (1999) suggests, rather indirectly, an environmental dependence of halo formation times. We revisit this argument in Section 4, noting that it also predicts the sign of the dependence, and predicts it correctly in the light of our results. The range of assumptions required for analytic theory to predict environmental independence also suggests that detection of some signal should be possible. To make progress on this matter using N -body simulations seems, then, to require one of two things. Firstly, we may try to pin down the environmental dependence of halo formation times suggested by the above results by using more sensitive tests. Sheth & Tormen (2004) claimed to have found such a test – the marked correlation function – and found a signal of environmental dependence despite using the same GIF simulations as Lemson & Kauffmann (1999). Marked statistics have recently proved useful in the analysis of both simulations (Faltenbacher et al. 2002; Gottlöber et al. 2002; Sheth, Connolly & Skibba 2006) and surveys (Beisbart & Kerscher 2000), offering both sensitivity and information complementary to that provided by other statistics. A more general discussion of marked statistics and their interpretation may be found in Sheth (2005). Secondly, we may use larger simulations, so that even a subset of the haloes spanning a small range in mass provides adequate statistical power to see significant evidence of environmental dependence, if this dependence exists and is sufficiently large to be interesting. Higher resolution would also allow us to study haloes which host only a single bright galaxy, so that we may hope for a more direct link between the halo properties and the galaxy properties than one would expect when studying more massive haloes. An environmental dependence of the merger histories of galaxy-sized haloes may provide a more direct explanation for the variation in galaxy properties with environment, and would suggest that the systematic change in the halo mass function with environment is not the only driving force behind the systematic change in galaxy properties with environment.

In this paper we attempt to combine both the above techniques. That is, we calculate the marked correlation function as suggested by Sheth & Tormen (2004), and later go on to discuss some other statistics closely related to the marked correlation function. We apply these calculations to the “Millennium Simulation” (Springel et al. 2005), which resolves the merger histories of haloes small enough that we expect them to host a single galaxy of lu-

minosity $0.1L_*$ (where L_* is the characteristic luminosity corresponding to the break in the galaxy luminosity function), but that probes a cosmologically representative volume. This is the simulation used by Gao, Springel & White (2005) to study the age-dependence of halo clustering, using an approach which is complementary to that taken here.

The structure of the paper is as follows. In Section 2 we describe the Millennium Simulation, and the merger trees used to calculate the formation times in this work. We describe the marked correlation function in Section 3. We also discuss here the choice of mark used for the majority of the results presented in this paper. Then in Section 4 we go on to describe our results, including tests to justify our choice of mark. These motivate the definition of a marked cross-correlation function, which we calculate for various halo samples. We also present results of a test of the effect of environment on halo formation time which corresponds more directly to earlier calculations using smaller simulations. Finally, we present our conclusions in Section 5.

Throughout we use the convention that the Hubble constant, $H = 100h \text{ km s}^{-1} \text{ Mpc}^{-1}$.

2 THE SIMULATION

In this study we use the Millennium Simulation (Springel et al. 2005) carried out by the Virgo Consortium using a modified version of the TREE-PM N -body code GADGET2 (Springel, Yoshida & White 2001b; Springel 2005). The cosmology is a flat, Λ CDM model, with $\Omega_m = 0.25$ (so $\Omega_\Lambda = 0.75$) and $h = 0.73$. The initial power spectrum was calculated using CMBFAST (Seljak & Zaldarriaga 1996), and is such that the primordial power spectrum has power-law index $n = 1$, the *rms* linear mass fluctuation in spheres of radius $8 h^{-1} \text{ Mpc}$ extrapolated to $z = 0$ is $\sigma_8 = 0.9$, and the baryon density is $\Omega_b = 0.045$. This leaves a dark matter density, $\Omega_{\text{dm}} = 0.205$. The simulation follows the evolution under gravity of 2160^3 dark matter particles in a periodic box with sides of comoving length $500 h^{-1} \text{ Mpc}$ from $z = 127$ to the present day. Each particle has mass $8.61 \times 10^8 h^{-1} M_\odot$, and the gravitational force has a Plummer-equivalent comoving softening length of $5 h^{-1} \text{ kpc}$. The particle data were output and stored at 64 times, 60 of which are spaced regularly in the logarithm of the expansion factor between $z = 20$ and $z = 0$, allowing the construction of trees detailing how each dark matter halo at $z = 0$ was built up through mergers and accretion.

2.1 Merger trees

At each of the output times of the simulation we have a catalogue of friends-of-friends groups (Davis et al. 1985) calculated using a linking length of $b = 0.2$ times the mean inter-particle separation. Locally overdense, self-bound substructures of these groups are found using the SUBFIND algorithm (Springel et al. 2001a). Each friends-of-friends halo is therefore decomposed into a collection of subhaloes, plus a fuzz of unbound particles. Of the subhaloes, one is typically much larger than the others and contains most of the mass of the halo. This can be thought of as the background mass distribution of the halo, while the smaller subhaloes are substructures.

Sometimes, however, the friends-of-friends algorithm links together structures which one might prefer to consider as separate haloes for the purpose of constructing the merger trees. Visually,

these haloes often appear to consist of two distinct structures joined by a tenuous bridge of particles. They may also be only temporarily joined, in the sense that following the evolution of the system would see the structures move apart and become distinct friends-of-friends haloes again. Having run SUBFIND, we identify these spuriously linked haloes as follows. We split a subgroup from its friends-of-friends halo before calculating the merger trees if either of the following conditions is satisfied: the centre of the subhalo is outside twice the half-mass radius of the main halo; or the subhalo has retained more than 75 per cent of the mass it had at the last output time at which it was an independent halo. The latter condition is imposed because we expect a less massive halo to be stripped of its outer layers as it merges with a more massive halo, while if it has been artificially linked by the friends-of-friends algorithm it will have retained most of its mass. Treating the subgroups which have been split off as separate haloes has also been found to lead to a better match between galaxy properties in SPH simulations and in semianalytic models which use the resulting merger trees (Helly et al. 2003b).

The splitting algorithm above results in a halo catalogue containing more haloes than in the original friends-of-friends catalogue. When we refer to a ‘halo’ below, we refer to a member of this new, larger catalogue. A halo, as before, is a collection of SUBFIND subhaloes including one background subhalo. Each halo in the catalogue at the final time has its own merger tree built from these catalogues. It has become conventional in studying the properties of the merger trees themselves, however, to calculate one merger tree per friends-of-friends halo, i.e. to define a halo as a friends-of-friends object. To provide contact with earlier work, therefore, if the splitting algorithm above results in a friends-of-friends halo being associated with two or more ‘merger tree haloes’ at the final time, we consider only the merger tree of the most massive component, and discard the other trees from the same halo in our analysis. The merger tree of this remaining component is unaffected by discarding the less massive components, since each subhalo at each redshift may appear in only one merger tree (in other words, if a halo or subhalo at some time has a descendant at a later time, as almost all haloes do, then this descendant is unique). Approximately 15 per cent of haloes are split in this way, and usually the mass of the discarded part is only a small fraction of the mass of the halo. The proportion of split haloes decreases with increasing halo mass, dropping to only a few per cent for haloes with mass close to the characteristic mass, M_* .

The merger trees are constructed from the group catalogues by following subhaloes from early times to late times, identifying in which halo a subhalo resides at the later time (Helly et al., in prep.). This means that given a subhalo in one snapshot, we must be able to find the corresponding object (the descendant subhalo) in a later snapshot. This is usually the next snapshot, though we check for a descendant in the next five outputs since occasionally friends-of-friends or SUBFIND are unable to identify the subhalo in the intervening snapshots. This may happen when, for example, a halo loses particles and drops below the resolution limit, or passes through a dense region in which it is not identified as a distinct object. The descendant of a subhalo is found by following the most bound 10 per cent of its mass or the 10 most bound particles, whichever is the greater mass. The descendant is the subhalo which contains the largest number of these particles. We identify the descendant of an entire halo as being the halo which contains the descendant of its most massive subhalo. Haloes therefore do not split: a halo at redshift z_1 has at most one descendant at redshift $z_2 < z_1$. If the particles of a halo do become distributed between

two haloes at a later time, only one of these two haloes may have the original halo as a progenitor. De-merger events may therefore lead to ‘orphan’ haloes with no progenitors. This physical splitting or de-merger of haloes as the simulation evolves is unrelated to the algorithm we use to split friends-of-friends haloes above. Clearly, though, our definition of a halo affects whether or not we consider two haloes to have de-merged, and we comment briefly on the impact of de-mergers on our results in Section 4.2.

Given a parent halo in the final snapshot, we call all haloes in earlier snapshots whose descendants are within the halo its progenitors. At each of the earlier snapshots, one of the progenitor haloes is designated the ‘main’ progenitor of the parent halo. This main progenitor is defined inductively as we move up in redshift one snapshot at a time as the most massive progenitor of the main progenitor in the previous snapshot. We then define the formation time of a halo as the redshift at which the main progenitor had half the mass of the final halo, linearly interpolating between the two redshifts at which its mass was greater than and less than half the final mass. This definition of formation redshift – the redshift at which the mass of the main progenitor falls below half the mass of the final halo – provides contact with analytic approaches to this problem and with earlier work on the formation time of N -body haloes (Lacey & Cole 1993; Sheth & Tormen 2004).

To calculate a marked correlation function of haloes we need to know the distance between any two haloes. We define this as the distance between their centres, and take the centre to be the position of the particle with the minimum gravitational potential energy, which is output by SUBFIND.

Finally, note that the trees used in this work were constructed independently of the Millennium Simulation merger trees discussed by Springel et al. (2005) and Gao et al. (2005). The two sets of trees differ both in the criteria for identifying independent haloes and in the treatment and identification of the descendant haloes themselves. In this respect, and in respect of the methods we use to analyse our halo catalogues, this work complements the study of the environmental dependence of halo formation by Gao et al. (2005). A discussion of the issues involved in constructing suitable merger trees (especially in the context of semianalytic models of galaxy formation) may be found in Helly et al. (2003a).

3 THE MARKED CORRELATION FUNCTION

Studying the dependence of halo formation time on halo environment requires, of course, a definition of halo environment. When using a dark matter simulation, a natural definition is the local overdensity in dark matter, measured on some chosen scale. This immediately highlights the problem of choosing an appropriate scale. It is not clear, for example, whether the choice of scale should depend on the mass of the halo under consideration. Then there are subsidiary choices such as whether to excise the region containing most of the mass of the halo from the region used to define the local overdensity.

Lemson & Kauffmann (1999) studied halo formation time as a function of the overdensity of dark matter in a spherical shell of inner radius $2 h^{-1}$ Mpc and outer radius $5 h^{-1}$ Mpc centred on the halo. There was no significant detection of a dependence of formation time on environment defined in this way. Sheth & Tormen (2004), however, proposed a test which they considered more sensitive, and which does not require a similar choice of scale. Their ‘marked correlation function’ is defined as follows.

Consider a set of N objects, taken in this case to be dark matter

haloes. To each one assign a ‘mark’ $\{m_i, i = 1, \dots, N\}$, where in this study we take the mark to be formation redshift, or some proxy for formation redshift. Let the pair $\{i, j\}$ have separation r_{ij} . Then the marked correlation function $\xi_{\text{marked}}(r)$, a function of separation r , is defined by

$$\xi_{\text{marked}}(r) = \sum_{\{i,j \mid r_{ij}=r\}} \frac{m_i m_j}{n(r) \bar{m}^2}, \quad (1)$$

where $n(r)$ is the number of pairs of objects with separation $r_{ij} = r$ and where the mean mark \bar{m} is calculated over all objects (of all separations) in the sample.

In other words, if $\xi_{\text{marked}}(r) > 1$ for some r then this implies that pairs of objects with separation r have a greater value of the mark than average. In the case of dark matter haloes, we expect that haloes in overdense environments have more close neighbours than haloes in underdense environments (some caveats to this interpretation are discussed in Section 4). Therefore the contribution of haloes in overdense environments dominates $\xi_{\text{marked}}(r)$ on small scales. On large scales, meanwhile, we expect to recover the global average, $\xi_{\text{marked}}(r) = 1$. If we see that $\xi_{\text{marked}}(r)$ deviates from 1 on some scale we may interpret this as an environmental dependence of the mark.

Note we do not have to choose a scale on which to study this dependence; the marked correlation function tells us the scale. This is clearly desirable, but comes at the cost that there is no straightforward correspondence between environment as defined by the marked correlation function and environment as defined by the overdensity in some region near the halo.

3.1 Choice of mark

In principle one could choose to measure the marked correlation function using any of a whole range of halo properties as the mark, in order to investigate the environmental dependence of those properties. Here, although we wish to study the environmental dependence of halo formation redshift, it may not be best to use this as the mark. Instead, for the majority of our results we follow Sheth & Tormen (2004) and use a ‘scaled formation redshift’ for our mark. The definition of scaled formation redshift, used here and in Sheth & Tormen (2004), is the $\tilde{\omega}_f$ parameter defined in equation 2.31 of Lacey & Cole (1993). Suppose we measure formation redshift relative to some final time z_0 (here, we always take $z_0 = 0$), and consider a halo with mass M_0 at z_0 and which formed at a redshift z_f . Then $\tilde{\omega}_f$ is given by

$$\tilde{\omega}_f = \frac{\delta_c(z_f) - \delta_c(z_0)}{\sqrt{\sigma^2(M_0/2) - \sigma^2(M_0)}}, \quad (2)$$

where $\delta_c(z)$ is the critical density threshold for collapse and $\sigma^2(M)$ is the linear theory variance of density fluctuations at mass scale M .

The motivation for using $\tilde{\omega}_f$ rather than z_f as the mark comes from the following predictions of extended Press–Schechter theory: firstly, that the distribution of $\tilde{\omega}_f$ depends very weakly on the initial power spectrum of fluctuations; and secondly, that for a power-law initial power spectrum, the distribution of $\tilde{\omega}_f$ is independent of halo mass. The latter prediction still holds to very high accuracy for more general power spectra with slowly varying slope. Moreover, the prediction is largely confirmed by measurement of the distribution in our simulation. This is demonstrated in Fig. 1, where the mean formation redshift of haloes in the Millennium simulation is plotted as a function of mass. For comparison, we plot the mean

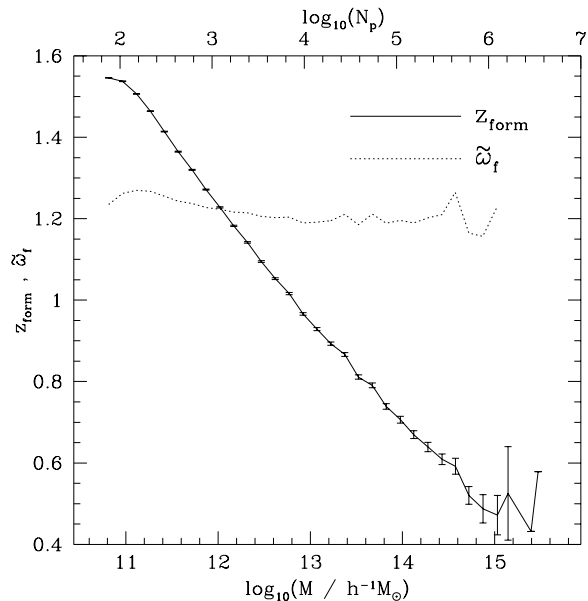


Figure 1. The solid line with error bars gives the mean formation redshift of haloes in the Millennium Simulation as a function of the mass of the halo (lower horizontal axis) or, equivalently, the number of particles in the halo (upper horizontal axis). The dotted line, which exhibits a much weaker mass dependence, shows on the same scale the mean value of the scaled formation redshift, $\tilde{\omega}_f$ (see Equation 2 for a definition), of haloes as a function of halo mass.

value of $\tilde{\omega}_f$ as a function of mass on the same scale. Clearly $\tilde{\omega}_f$ scales out much of the dependence of halo formation redshift on halo mass.

This can be seen in more detail by comparing Fig. 2a, which shows the distribution of formation redshift for haloes in different mass bins in the simulation, with Fig. 2b, which shows the distribution of $\tilde{\omega}_f$ for the corresponding haloes. In Fig. 2a we can easily see that haloes of different masses have very different distributions of formation redshift, and that there is a clear trend of larger mass haloes having a more strongly peaked distribution with a peak at smaller redshift. In Fig. 2b, however, we see that the distribution of $\tilde{\omega}_f$ is quite similar for haloes of different mass, and that there is no such clear trend. Fig. 2b also shows the analytic prediction for this distribution, which can be seen to be a reasonable approximation. The analytic form captures the shape of the distribution well, though it appears to predict a distribution peaking at smaller $\tilde{\omega}_f$. We show both the analytic distribution calculated using the actual input power spectrum of the Millennium Simulation, and the closed form for a power-law initial power spectrum with index $n = 0$ (Lacey & Cole 1993). Note the very weak dependence of the distribution on power spectrum.

The main benefit of defining our mark in this way is that we may now be justified in calculating the marked correlation function for a set of haloes which span a broad range in mass, thereby utilising the full statistical power of our simulation. Such a function would not have been easy to interpret using z_f as the mark, since it is well established that the halo mass function depends on local density: in high-density regions, it becomes skewed towards more massive haloes (Frenk et al. 1988; Cole & Kaiser 1989; Lemson & Kauffmann 1999; Gottlöber et al. 2003; Mo et al. 2004). Because these more massive haloes tend to have formed more recently, we could not have been sure that any signal in the

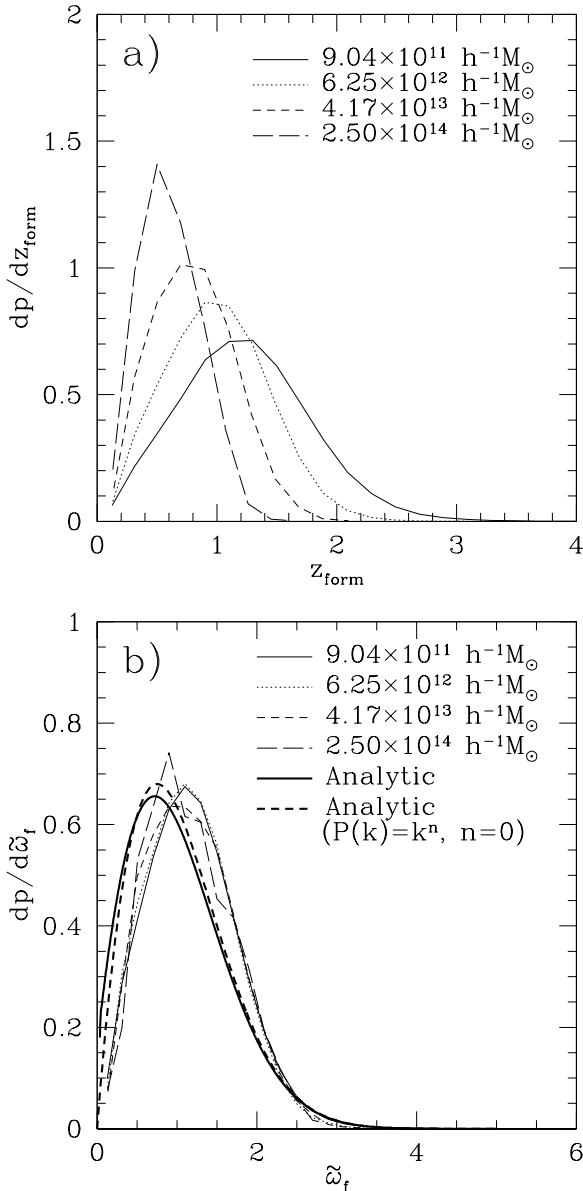


Figure 2. The distribution of halo formation redshift (top panel) and of scaled formation redshift $\tilde{\omega}_f$ (bottom panel). The distribution is shown for haloes in four different mass bins spaced equally in $\log(\text{halo mass})$ and centred on the mass given in the legend. The trend in the top panel is such that haloes of larger mass have a more strongly peaked distribution, with the peak at smaller redshift. In the bottom panel, we show in addition the analytic prediction for the distribution of $\tilde{\omega}_f$ (which is very nearly independent of mass) with thicker, smoother lines. The thick, solid line shows the prediction using the input power spectrum for the Millennium Simulation, while the thick, dashed line shows the prediction using a power-law initial power spectrum with index $n = 0$.

marked correlation function was not due merely to the environmental dependence of the mass function, rather than of mean halo formation redshift for haloes of a given mass. This effect could also have swamped any genuine signal from an environmental dependence of formation time.

4 RESULTS AND EXTENSIONS

A calculation of the marked correlation function of haloes with mass between $3.11 \times 10^{12} h^{-1} M_{\odot}$ and $3.11 \times 10^{14} h^{-1} M_{\odot}$ at $z = 0$ is given in Fig. 3a (our results will be for $z = 0$ throughout). We write the halo mass in terms of the characteristic mass M_* , where M_* is defined in the usual way such that $\sigma(M_*) = \delta_c$, and where $\delta_c(z = 0) = 1.674$ for the cosmology assumed here. M_* haloes are both well resolved and numerous, containing 7221 particles and having a mass of $6.21 \times 10^{12} h^{-1} M_{\odot}$ at $z = 0$ in the Millennium Simulation. The peak in the function at intermediate scales indicates that haloes in pairs with these separations have a mean formation redshift which is higher than the global average for haloes of this mass. The function tends to 1 at large scales, as expected. At smaller scales than those plotted, i.e. less than approximately $1 h^{-1}$ Mpc, the marked correlation function is not defined for haloes of this mass, since there are no pairs of haloes in this mass range at such small separations. Clumps of mass closer than this will tend to be identified as part of the same structure by the group-finder.

The sense of the dependence (higher formation redshifts in denser regions) is that predicted by Sheth & Tormen (2004) from the results of Lemson & Kauffmann (1999). They noted that when the distribution of formation times (averaged over haloes of all mass) was plotted for haloes residing in regions of different overdensity (measured in a spherical shell between 2 and $5 h^{-1}$ Mpc centred on the halo), the curves were very similar, i.e. the distribution of halo formation redshifts was independent of local density. This seems inconsistent with the fact that denser regions tend to host more massive haloes, which have, on average, more recent formation times (see Fig. 1). One might expect that because the distribution is calculated by averaging over all haloes for each bin in overdensity, the distribution should shift to lower formation redshifts in more dense regions, but this was not observed. This could be explained if haloes of a given mass tend to have higher formation redshifts in more dense regions. No such signal was observed in the GIF simulations, which motivates the use of a more sensitive test of environmental dependence. It also suggests using simulations of larger volume, since while the volume of the GIF simulations may have been sufficient to detect a variation in the distribution of formation times when averaging over haloes of all masses, it was not sufficient for Lemson & Kauffmann (1999) to detect a variation in the mean formation redshift as a function of local overdensity for haloes in some narrow range in mass. The Millennium Simulation offers the opportunity to do this (and to extend the study to haloes of lower mass) and we do so in Section 4.2.

Rather than plot error bars on the (correlated) points of Fig. 3a, we attempt to assess the significance of any signal similarly to Sheth & Tormen (2004). That is, we take the population of haloes used to calculate the marked correlation function, then shuffle their marks randomly and recalculate the marked correlation function 100 times. For each radial bin, we calculate the mean of these 100 realizations of the marked correlation function and the standard deviation between realizations. The mean plus or minus one standard deviation is given by the dotted lines.

We have also tried to quantify the systematic error induced by including haloes over such a large mass range. We repeat the procedure used to obtain the dotted lines of Fig. 3a, but instead of shuffling marks over our entire sample of haloes, we sort the haloes into eight mass bins. Then we only shuffle the marks within each bin in mass. Therefore, although a halo receives the mark of a random halo in the sample, it is only permitted to receive the mark of a

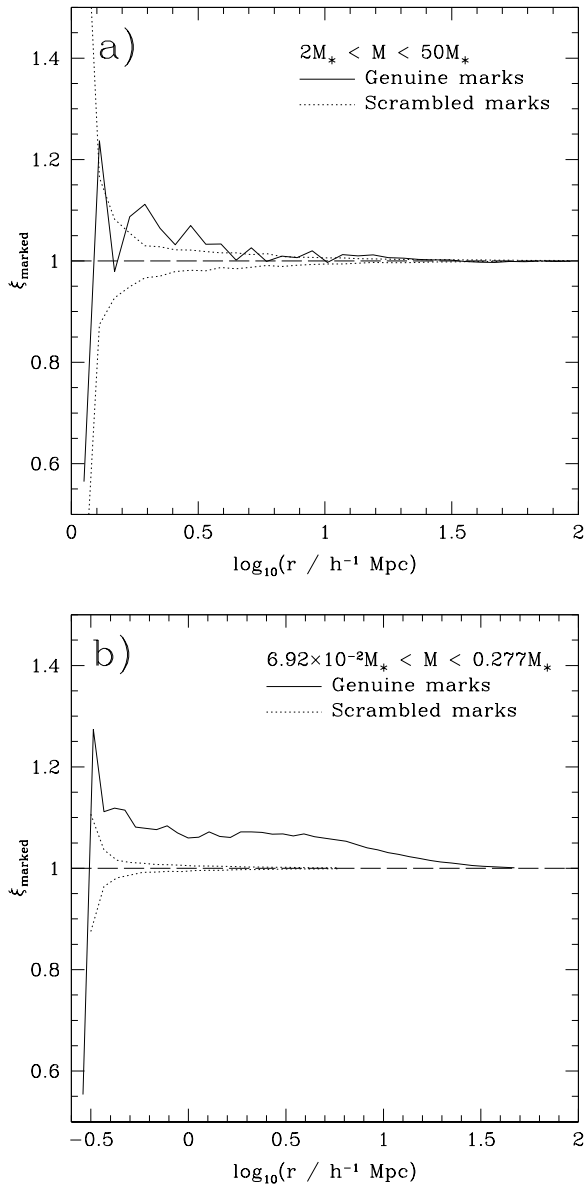


Figure 3. The marked correlation function (using $\tilde{\omega}_f$ as the mark) of haloes with mass, M , in the range shown (solid line). In the top panel, this corresponds to haloes with a number of particles, N_p , such that $14\,441 \leq N_p \leq 361\,036$ (there are 7221 particles in an M_* halo). There are 34 241 haloes in this mass range in the Millennium Simulation. In the bottom panel, the haloes have between 500 and 2000 particles. These haloes have a mass such that we typically expect them to host a single bright galaxy.

halo with a very similar mass. We then take the mean and standard deviation in each radial bin of the realizations of the marked correlation function as before. This binning procedure makes very little difference, in fact, and gives us confidence that the $\tilde{\omega}_f$ parameter scales out the mass dependence of halo formation redshifts sufficiently well for the purposes of this test.

To give a numerical indication of the strength of the signal, we calculated the marked correlation function in one large bin between 1 and $5 h^{-1}$ Mpc and estimated the error using the same shuffling procedure as before. This indicated that the value of ξ_{marked} was

inconsistent with unity at the 5σ level. It is the large volume of our simulation which enables us to see a signal in the marked correlation function of such massive haloes, but we find that the behaviour of samples of haloes of lower mass is similar. Moreover, the dynamic range of the simulation is such that we can study relatively small haloes, robustly determining formation times of haloes down to a mass of $5.5 \times 10^{10} h^{-1} M_\odot$. For galaxy-sized haloes with between 500 and 2000 particles, for example, we see a larger environmental dependence. The marked correlation function for haloes of this mass is given in Fig. 3b. The abundance of haloes of this mass means that the error in the determination of the marked correlation function is negligible at most scales of interest. The excess at small separations is more significant than for the more massive haloes, and the size of the effect is also larger. This is qualitatively consistent with Gao et al. (2005) since the effect for which they tested (a variation in clustering amplitude with halo formation redshift) was larger for haloes of lower mass.

Splitting the mass range used in Fig. 3a into four parts gives the result shown in the lower four panels of Fig. 4. Firstly, it is clear that the estimates of ξ_{marked} in Fig. 4 are far more noisy; while the mass range covered in Fig. 3a contains 34 241 haloes in the Millennium Simulation, the lower four panels of Fig. 4 cover mass ranges containing, in order of increasing mass, 18 384, 9172, 4298 and 2387 haloes respectively. Since the quality of the statistics is governed by the number of halo *pairs*, the effect is noticeable even given the large volume of the simulation. This highlights the importance of properly scaling out the mass dependence of halo formation redshift, so that we may average over large ranges in halo mass.

For similar reasons, (i.e. the effect of cross-correlations between bins) the marked correlation function for the whole mass range of Fig. 3a is not simply the average of the marked correlation function of each of the four sub-ranges. For example, if we perform the test described above of calculating the marked correlation function for one large bin between 1 and $5 h^{-1}$ Mpc, we see that the function for the range $2M_* < M < 4M_*$ is greater than unity only at the 1σ level. In the highest mass range, the function in this radial bin is less than unity, by approximately 1.5σ . One would normally dismiss this apparent change in the sign of the environmental dependence as insignificant, especially given our free choice of bin size and the freedom in the definition of the halo catalogue and merger trees, but it is qualitatively consistent with fig. 4 of Sheth & Tormen (2004). In the amalgamated sample, of course, most of the halo pairs which include a member in the highest mass bin have one member of the pair from a lower mass bin. It may therefore still be the case that the product of the marks of the haloes in such a pair with separation r is usually greater than \bar{m}^2 , and yet a halo pair of separation r in which both members are from the highest mass bin usually gives a product of marks less than \bar{m}^2 . This is a barrier to the clean interpretation of these results, since when measuring the environmental dependence of haloes in some mass range, the environment can only be defined in terms of haloes in the same mass range. We address this problem by explicitly separating the ‘tracer’ population from the ‘marked’ population in Section 4.1 below.

Recall that the small-scale cutoff in the marked correlation function occurs because there are no haloes in the given mass range which occur at such small separations in the simulation: an exclusion effect. The radius at which this occurs depends on mass, and certainly this effect is noticeable when comparing the top-left panel of Fig. 4 to the bottom-right panel.

This dependence on halo mass of the scale upon which we

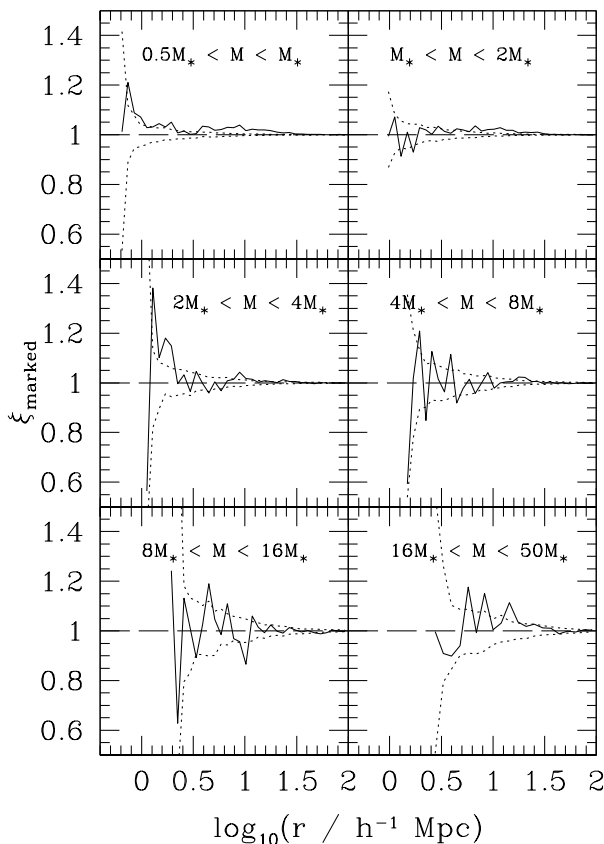


Figure 4. The marked correlation function of haloes with mass in the ranges shown (solid lines), with $\tilde{\omega}_f$ as the mark. Dotted lines are calculated as in Fig. 3a. The top four panels may be compared with fig. 4 of Sheth & Tormen (2004) since the value of M_* in their simulation is approximately twice ours. Note, though, the difference in axis scale, and the fact that in their figure formation redshift is used for the mark, whereas here $\tilde{\omega}_f$ is used (see Fig. 5 which shows this does not affect our conclusions). The lower four panels cover the same mass range as Fig. 3a.

can measure environment again suggests separating the tracer and marked populations, as we do when calculating a marked cross-correlation function below. Of course, some dependence is inevitable since more massive haloes tend to have larger radii. This reinforces the point that a method in which we choose beforehand a fixed scale on which to measure environment – looking at scales at which there is a peak in the marked correlation function for low mass haloes, say – may be flawed, since the outer regions of more massive haloes will contribute to the definition of their own environment.

We emphasized earlier the importance of being able to calculate a marked correlation function for a sample of haloes which spans a large range in mass, and suggested a scheme for scaling out the mass dependence of halo formation times based on the analytic work of Lacey & Cole (1993). One can easily imagine other ways to scale out this dependence, however, and we attempt to show the difference between various methods in Fig. 5. For the solid line we make no attempt to correct for the mass dependence of halo formation redshift and simply use z_f as the mark, while for the other three lines some kind of scaling is applied. The short-dashed line is the result for our fiducial mark, $\tilde{\omega}_f$. The dot-dashed line uses

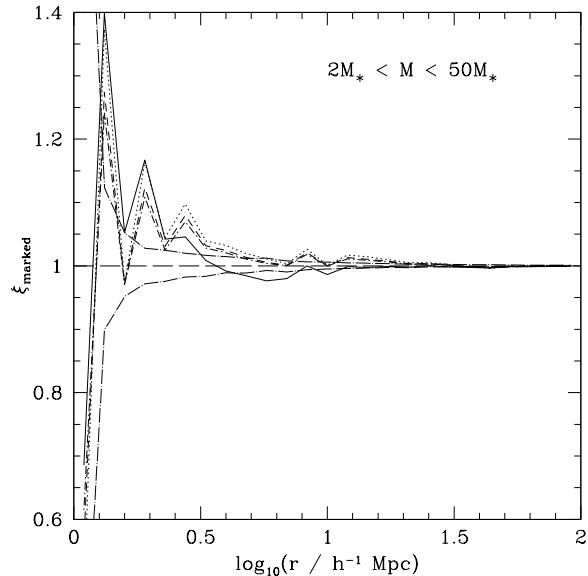


Figure 5. The marked correlation function with several different choices of mark. In each case the population of haloes used is the same as in Fig. 3a, but we vary the choice of mark as follows: solid line – formation redshift; short-dashed line – $\tilde{\omega}_f$; dot-dashed line – formation redshift divided by the mean formation redshift for haloes of that mass (determined from the simulation); dotted line – haloes are ranked by $\tilde{\omega}_f$ then reassigned a mark (preserving this ranking) such that the marks follow the analytic distribution for $\tilde{\omega}_f$ given by the thick, solid line in Fig. 2b. The long-dashed line through $\xi_{\text{marked}} = 1$ is shown to guide the eye. The dispersion in ξ_{marked} in the scrambled catalogues is shown only for a mark of $\tilde{\omega}_f$ (dot-long-dashed lines), since it is very similar in each case.

the simulation itself to determine the scaling: we simply divide the formation redshift for each halo by the mean formation redshift for haloes of that mass. This does not take into account changes in the shape of the distribution of formation redshift as a function of mass. For the dotted line we first calculate $\tilde{\omega}_f$ for each halo, as above. Then we rank the haloes in order of $\tilde{\omega}_f$ and reassign each one a mark, preserving the ranking, such that the final distribution of marks is precisely the analytic distribution given by the thick, solid line of Fig. 2b. This explicitly enforces near-mass independence, hopefully without distorting the shape of ξ_{marked} too much since the shape of the analytic distribution matches the measured distribution quite well. It seems from Fig. 5 that any reasonable method for scaling out the mass dependence of the distribution of halo formation redshift gives similar results.

The errors in the marked correlation functions measured with these four different marks are very similar, and the effect of shuffling only within narrow mass bins remains small in each case. Indeed, when we force the marks to follow the analytic distribution for $\tilde{\omega}_f$ we might expect it to make no difference whether we shuffle between haloes of all masses or only between haloes of similar mass, and we have checked that this is indeed the case. Fig. 5 gives us confidence that our conclusions about the environmental dependence of halo formation redshift are robust to changes in the precise definition of the mark, so long as the mark remains a reasonable proxy for the halo formation redshift as defined in Section 2.1, and so long as the width of the distribution of marks remains similar. We conclude, therefore, that we have significant evidence that halo

formation redshift does depend on environment, and we explore this in more detail in what follows.

4.1 A marked cross-correlation function

Even the marked correlation functions we calculate above which include haloes in a wide range of mass (up to a factor of about 25 between the lowest and highest mass) utilise only a fraction of the dynamic range available in the Millennium Simulation. We are more limited by the fact that the wider the range of mass studied, the harder the marked correlation functions are to interpret. If we include very small haloes, then because low mass haloes are more abundant, the function will be dominated at all scales by contributions from low mass haloes. The contribution from haloes of any given mass only cuts in above some scale determined by the exclusion effect from the non-zero size of the halo. On the other hand, if we wish to study the environmental dependence of the formation times of only very massive haloes, we will have poor statistics even when simulating enormous volumes, and it will not be clear in any case that such massive haloes are good tracers of environment. We have attempted to address some of these problems by defining a marked cross-correlation function.

Consider two populations of haloes, which we denote the ‘tracer’ population and the ‘marked’ population. We then define the marked cross-correlation function, $\xi_{\text{marked}}^{\text{cross}}(r)$, by

$$\xi_{\text{marked}}^{\text{cross}}(r) = \sum_{\{i,j \mid r_{ij}=r\}} \frac{m_j}{n(r)\bar{m}} \quad , \quad (3)$$

where the sum is now taken over pairs $\{i,j\}$ such that halo i is from the tracer population and halo j is from the marked population, $n(r)$ is the number of such pairs of separation r and \bar{m} is the mean mark of the haloes in the marked population. This tells us about the environmental dependence of the mark in the marked population, with environment defined in terms of the tracer population. It retains the property that a deviation of the function from unity indicates environmental dependence. Note, however, that it does not have some of the properties of a normal cross-correlation function: it will be different if we exchange the marked and tracer populations, and the marked cross-correlation function of a population with itself is not equivalent to the marked autocorrelation function.

Fig. 6 gives six examples of marked cross-correlation functions with $\tilde{\omega}_f$ as the mark. We estimate the dispersion among realizations of the functions by recalculating the function 100 times with the marks shuffled, as before. The tracer population is the same in each panel, but the mass of the marked population increases from left to right and from top to bottom. For the higher mass populations there seems to be a trend that as the mass of the marked population increases, the positive signal from the marked cross-correlation function becomes weaker, perhaps even changing sign when the mass of the marked haloes becomes greater than that of the tracer haloes. Since we expect individual L_* galaxies to occupy haloes containing approximately 1000 particles in this simulation (a halo with 1000 particles has a mass of $0.138M_* = 8.61 \times 10^{11} h^{-1} M_\odot$), the results for lower mass populations suggest we have significant evidence that galaxy-sized haloes near $6 \times 10^{13} h^{-1} M_\odot$ haloes have earlier formation times than the mean.

Comparing to the marked autocorrelation function, then, the most puzzling panels of Fig. 6 are the lower right panel and, to a lesser extent, the lower left panel. The trend in the marked cross-correlation function in the lower right panel is in the opposite sense

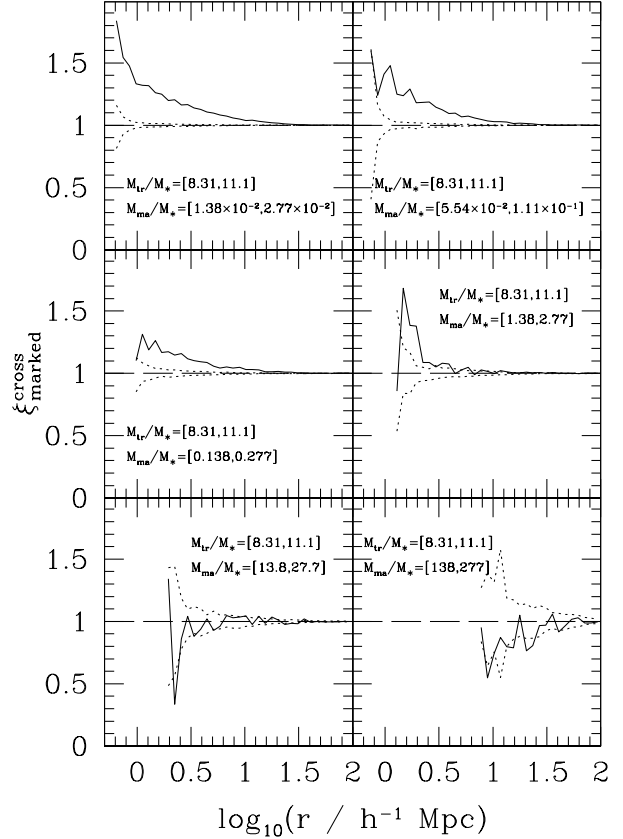


Figure 6. Solid lines show the marked cross-correlation function of haloes with the same tracer population ($6 \times 10^{13} h^{-1} M_\odot$ haloes) each time, but with a marked population of different mass in each panel. The mark is $\tilde{\omega}_f$. The haloes in the tracer population have mass M_{tr} in the range shown, while those in the marked population have mass M_{ma} in the range shown (recall an M_* halo contains 7221 particles, and a galaxy-sized, 1000 particle halo has mass $0.138M_*$). We again show the dispersion in 100 calculations of the marked cross-correlation function (dotted lines), shuffling the marks at random between haloes each time.

to that which one may expect having seen the earlier results (less than unity at $\sim 2.5\sigma$ for one bin between 5 and $30 h^{-1} \text{ Mpc}$), while we see no signal in the lower left panel. Recall that we expect more close pairs in more dense regions. This means the marked correlation function at small scales is representative of dense regions, so that we expect to see earlier formation times. This expectation may not hold in the situation represented by the lower right panel of Fig. 6, however. While the tracer population consists of haloes with mass near $6 \times 10^{13} h^{-1} M_\odot$, the marked population in this panel consists of very massive haloes, of around $10^{15} h^{-1} M_\odot$. These large haloes will be found only in regions which are at least moderately dense, and many will be found in the very densest parts of the simulation: in the core of the filaments making up the cosmic web, or at the intersection of the filaments. In these highly dense regions, we expect nearby haloes to also be very massive, whereas it is in the moderately dense regions that $6 \times 10^{13} h^{-1} M_\odot$ haloes are most abundant. It may be that by choosing this tracer population, the close pair counts are dominated by haloes in only moderately dense regions, since it is here that our tracer population is most abundant. The large-scale pair counts are more representa-

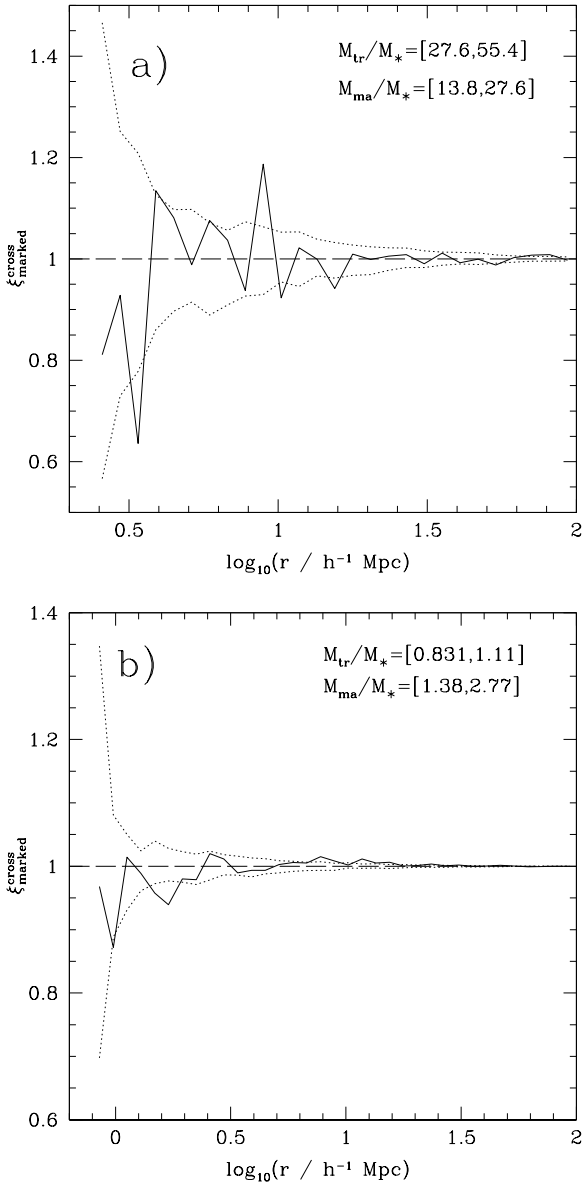


Figure 7. The top panel shows the marked cross-correlation function using the same marked population as the lower-left panel of Fig. 6. Here, though, we choose the tracer population to be more massive than in Fig. 6, and, importantly, more massive than the marked population. The dotted lines are as in Fig. 6. The bottom panel uses the same marked population as the middle-right panel of Fig. 6 but with a lighter tracer population.

tive of the average environment of $10^{15} h^{-1} M_{\odot}$ haloes, which is even more dense. If this interpretation is correct, we might anticipate that using a more massive tracer population would reverse the trend, so that $\xi_{\text{marked}}^{\text{cross}}(r)$ was once again larger on small scales. We test this prediction in Fig. 7a. In this figure the marked population is the same as in the lower-left panel of Fig. 6, since this allows us to choose a sufficiently abundant tracer population that is nevertheless more massive than the marked population.

While the signal we see in Fig. 7a is weak and more noisy (with only 872 haloes in the tracer population and 2189 haloes in the marked population) there is no repetition of the unexpected trend seen in the lower panels of Fig. 6. We have also performed the

converse test, in Fig. 7b. That is, we take the marked population that produces a positive signal in the middle right panel of Fig. 6, and find the marked cross-correlation function of these haloes with a less massive tracer population. Using lower mass haloes also improves our statistics: there are 26 417 and 20 968 haloes in the tracer and marked population respectively. The positive signal seen in Fig. 6 at small scales is wiped out, and if anything there is a weak negative signal. This suggests that a definition of environment using some tracer population only really corresponds with our intuition of what environment should mean (close pairs representing a dense environment) if the tracer population is at least as strongly clustered as the marked population.

4.2 A simpler test of environment

Having seen evidence of environmental dependence of halo formation times in the marked correlation function, it is interesting to see whether the volume and dynamic range offered by the Millennium Simulation allow us to see a signal in other measures of environment. For Fig. 8 our measure is simply the overdensity in dark matter in a spherical shell between 2 and $5 h^{-1}$ Mpc from the centre of the halo (where the centre is defined, as before, as the position of the particle in the main substructure of the halo having the least gravitational potential energy). This is the same measure as used in fig. 3 of Lemson & Kauffmann (1999) in which no signal is apparent, despite the simulation being the same as the one which showed evidence of environmental dependence in the marked correlation function analysis of Sheth & Tormen (2004): both studies used the GIF simulations (Jenkins et al. 1998; Kauffmann et al. 1999). The range in halo mass used for each panel of our plot is the same as in fig. 3 of Lemson & Kauffmann (1999). A clear trend is visible; for the top three panels especially, there is evidence that haloes in regions with overdensities greater than about 1 or 2 have higher formation redshifts. We can follow this trend over a very wide range in overdensity.

Because of the high resolution of our simulation, we may extend this technique to lower mass haloes. Haloes which are expected to host a single, bright galaxy (and – importantly for this analysis – the progenitors of these haloes) are well resolved, containing roughly 1000 particles. Fig. 9 is similar to a single panel of Fig. 8, but using haloes with between 500 and 2000 particles, corresponding to masses of between 4.30×10^{11} and $1.72 \times 10^{12} h^{-1} M_{\odot}$. It is clear we have very significant evidence that haloes in denser regions have higher formation redshifts than the mean, and conversely that haloes in less dense regions have lower formation redshifts than the mean. The size of the effect is similar to that for the more massive haloes (larger, if anything – consistent with Gao et al. (2005)), but is detected more cleanly due to the large sample size. Reproducing Figs 8 and 9 using $\tilde{\omega}_f$ as a proxy for formation redshift gives extremely similar results. The mean is slightly offset, as one would expect from Fig. 1, but the trends are identical.

The dispersion in formation times at a given overdensity is larger than the systematic variation between different overdensities. Therefore it is unclear from these data what the effect of this variation will be on, for example, the properties of the central galaxies hosted by these haloes. Gao et al. (2005) use the Millennium Simulation to address the question of how the clustering of haloes of a given mass depends on their formation time, and find a clear difference between the clustering of the oldest and youngest haloes. We do not yet know the effect of this difference on observables such as the galaxy correlation function (split by colour or galaxy envi-

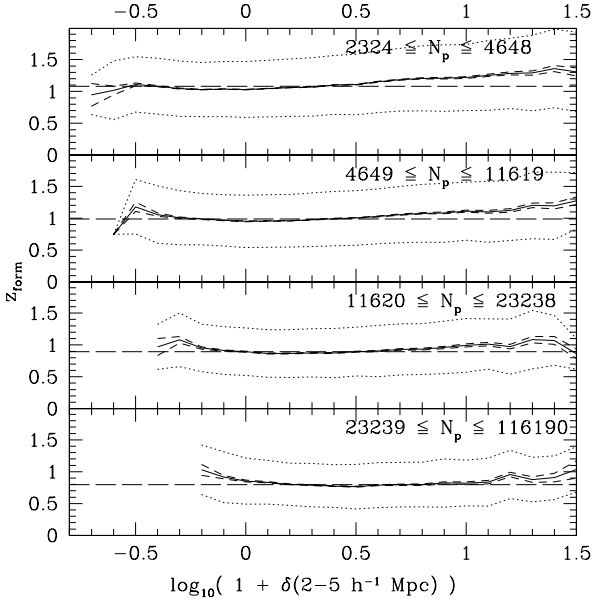


Figure 8. The formation redshift of haloes as a function of overdensity in a spherical shell of inner radius $2 h^{-1}$ Mpc and outer radius $5 h^{-1}$ Mpc centred on the halo (solid lines). The range of particle numbers for the haloes in each panel is shown; these are chosen so that haloes have the same mass as those in the corresponding panel of fig. 3 of Lemson & Kauffmann (1999). Note the difference in the scale of the horizontal axis between the linear scale of fig. 3 of Lemson & Kauffmann (1999) and the logarithmic scale of this figure which extends to higher densities. Short-dashed lines show the error on the determination of the mean formation redshift in each bin in overdensity. Dotted lines show the $1\text{-}\sigma$ dispersion in halo formation times. The flat, long-dashed line is at the mean formation redshift for all haloes in that bin in mass, and is shown only to guide the eye.

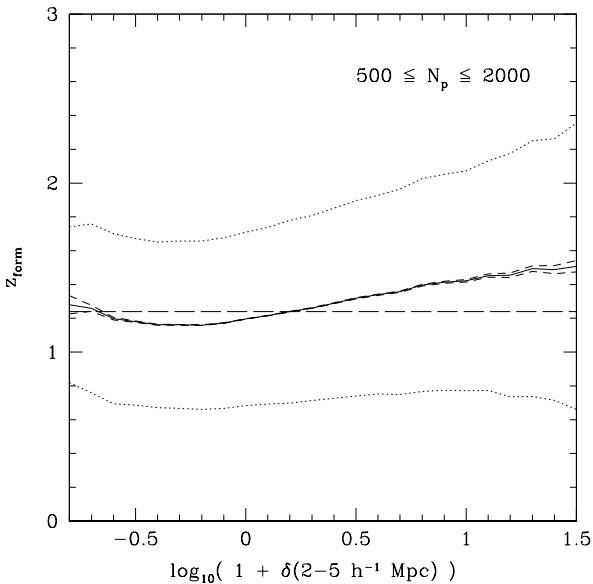


Figure 9. As Fig. 8, but for haloes with mass such that we may expect them to host a single bright galaxy. The halo sample is the same as for Fig. 3b.

ronment), especially in the light of the fact that galaxies of a given luminosity reside in haloes with a range of mass, with most galaxy light expected to come not from single-occupation haloes such as these, but from group-sized haloes (Eke et al. 2005). This problem may be addressed by galaxy catalogues constructed using the halo catalogues and merger trees from the Millennium Simulation (e.g., Bower et al. 2006; Croton et al. 2006).

In Fig. 9, the mean formation redshift crosses from being below the global mean for haloes in this mass range (long-dashed line) to above it at an overdensity $\delta \approx 0.6$. It appears this crossing point moves to higher overdensity for more massive haloes: in the bottom panel of Fig. 8 the crossing point is at $\delta \approx 5$. We have repeated these calculations and our marked correlation function calculations using different halo catalogues and merger trees, including those of Gao et al. (2005). While the position of this crossing point and the precise shape of the curve are sensitive to the detailed definition of the halo catalogues and the merger trees, the general trends are robust.

Performing the calculations of Gao et al. (2005) using our trees, or our marked correlation function analysis using their trees, gives qualitatively consistent results. This is encouraging since the two sets of trees are constructed quite differently, though using the same SUBFIND catalogue. For example, they define the formation time using the mass within r_{200} (the radius at which the enclosed density falls below 200 times the critical density), whereas we use the mass of the friends-of-friends halo. Also, to find the merger tree of a friends-of-friends halo they follow only the merger history of its main substructure, while we follow the combined histories of each of the substructures which make up the halo. This allows Gao et al. (2005) to track more easily the history of a halo which was temporarily the substructure of a larger halo, but which has since de-merged to become a separate halo in its own right. It is important to deal with these de-mergers well, since they lead to close pairs in dense environments in which one member of the pair is likely to be unusual in some way: for example, it may be assigned an artificially low formation redshift. We note in Section 2.1 that we take precisely one merger tree per friends-of-friends halo, discarding the lower mass trees which were split off having been deemed to have been spuriously connected. Including these trees causes de-merger problems since merger tree haloes can split despite remaining in the same friends-of-friends halo. On the other hand, using merger trees constructed purely from friends-of-friends catalogues without identifying substructure causes even greater problems, since haloes are often spuriously attached and subsequently split. So long as we take these de-mergers into account, all our results remain robust to the precise definition of the halo catalogue or the merger trees.

5 CONCLUSIONS

In this paper, we have looked for evidence of an environmental dependence of halo formation times, using what we consider to be an especially sensitive test, and using a very large simulation which offers excellent statistical power when constraining the properties of haloes with a large range of mass. We have very strong evidence that haloes of a given mass in denser regions formed at higher redshift than those in less dense regions. This result is robust to changes in the mark used as a proxy for formation redshift, and we conclude that the observed dependence is not affected by systematic bias from averaging over a range of halo mass. Our conclusions

are also unaffected by the precise definition of the halo catalogue or by the details of the construction of the merger trees.

Separating the haloes for which we wish to measure environment from those used to define environment allows us to look for the origin of the signal in more detail. We see a stronger dependence on environment for low mass haloes, although the effect is still present when more massive haloes are considered. We also note that in this context it only makes sense if the environment of low mass haloes is traced by a population of higher mass haloes. Using numerous, low mass haloes to trace the environment of more massive haloes means that our definition of environment may no longer correspond to an intuitive definition, in that it may no longer be the case that a relatively large number of close neighbours implies a relatively dense environment.

If we revert to a more intuitive test of the dependence of formation time on environment, and look at the mean formation redshift of haloes of a given mass as a function of the local overdensity in dark matter, we note that the size and resolution of our simulation allows us to see a highly significant signal of environmental dependence for haloes with a wide range in mass, but again especially for low mass haloes. We are able to perform this test for haloes which we expect to host only a single, bright galaxy, since the progenitors of these haloes are well resolved. The size of the variation in mean formation redshift is smaller than the (large) dispersion in formation redshift for haloes residing in a region of given overdensity. This makes the impact of this dependence on statistics such as the galaxy correlation function unclear, though this effect is studied in more detail by Gao et al. (2005) (who used the same simulation but different merger trees) where the age dependence of halo clustering is studied and a significant signal is observed.

Our results have, in any case, some implications for galaxy formation models and for halo models of clustering. Any simple version of the halo occupation distribution formalism (Seljak 2000; Berlind & Weinberg 2002; Cooray & Sheth 2002), for example, has as one of its basic assumptions that knowing the mass of a halo is sufficient to statistically determine the properties of its galaxy population. So long as the properties of the galaxy population depend sufficiently strongly on the merger history of a halo, we see that this assumption is no longer strictly valid, and this therefore calls into question the validity of results based on this formalism (e.g., Berlind et al. 2003; Abazajian et al. 2005). While extended Press-Schechter theory does a reasonable job of predicting the distribution of halo formation redshifts when averaging over haloes in all environments, it also predicts that the formation history is independent of environment. We clearly see that this is not the case, so the practice of assigning a Monte Carlo merger tree constructed according to extended Press-Schechter theory to a simulated halo based only on the halo mass is called into question. The magnitude of this effect on any observables drawn from mock galaxy catalogues generated by semi-analytic models using these merger trees is unclear at this stage, and may only become clear when comparing catalogues produced using Monte Carlo merger trees with those produced using merger trees extracted directly from the simulation being populated. This latter approach has become feasible with the advent of simulations of sufficient resolution and volume, such as the Millennium Simulation used here. It may still be the case that the width of the distribution of formation redshifts in a given environment, and the scatter in other relations such as the halo mass – central galaxy luminosity relation, wash out this effect. Uncertainties in the galaxy formation models themselves may prove to be more important. Equally, though, if other halo properties such as the concentration and angular momentum depend strongly enough

on formation time or environment, then this may help the models to better match and explain observations of the environmental dependence of galaxy colour and morphology, or the concentration or velocity profiles of galaxies of different ages.

ACKNOWLEDGEMENTS

GH acknowledges receipt of a PhD studentship from the Particle Physics and Astronomy Research Council. The simulation used in this paper was carried out as part of the programme of the Virgo Consortium on the Regatta supercomputer of the Computing Centre of the Max-Planck-Society in Garching.

REFERENCES

- Abazajian K. et al., 2005, *ApJ*, 625, 613
 Balogh M., Eke V., Miller C., Lewis I., Bower R., Couch W., Nichol R. et al., 2004, *MNRAS*, 348, 1355
 Bardeen J. M., Bond J. R., Kaiser N., Szalay A. S., 1986, *ApJ*, 304, 15
 Beisbart C., Kerscher M., 2000, *ApJ*, 545, 6
 Berlind A. A., Weinberg D. H., 2002, *ApJ*, 575, 587
 Berlind A. A. et al., 2003, *ApJ*, 593, 1
 Bond J. R., Cole S., Efstathiou G., Kaiser N., 1991, *ApJ*, 379, 440
 Bower R. G., 1991, *MNRAS*, 248, 332
 Bower R. G., Benson A. J., Malbon R., Helly J. C., Frenk C. S., Baugh C. M., Cole S., Lacey C. G., 2006, *MNRAS*, submitted (astro-ph/0511338)
 Cole S., Aragon-Salamanca A., Frenk C. S., Navarro J. F., Zepf S. E., 1994, *MNRAS*, 271, 781
 Cole S., Kaiser N., 1989, *MNRAS*, 237, 1127
 Cole S., Lacey C. G., Baugh C. M., Frenk C. S., 2000, *MNRAS*, 319, 168
 Cooray A., Sheth R., 2002, *Physics Reports*, 372, 1
 Croton D. J. et al., 2006, *MNRAS*, 365, 11
 Davis M., Efstathiou G., Frenk C. S., White S. D. M., 1985, *ApJ*, 292, 371
 Dressler A., 1980, *ApJ*, 236, 351
 Eke V. R., Baugh C. M., Cole S., Frenk C. S., King H. M., Peacock J. A., 2005, *MNRAS*, 362, 1233
 Faltenbacher A., Gottlöber S., Kerscher M., Müller V., 2002, *A&A*, 395, 1
 Frenk C. S., White S. D. M., Davis M., Efstathiou G., 1988, *ApJ*, 327, 507
 Gómez P. L. et al., 2003, *ApJ*, 584, 210
 Gao L., Springel V., White S. D. M., 2005, *MNRAS*, 363, L66
 Gottlöber S., Lokas E. L., Klypin A., Hoffman Y., 2003, *MNRAS*, 344, 715
 Gottlöber S., Kerscher M., Kravtsov A. V., Faltenbacher A., Klypin A., Müller V., 2002, *A&A*, 387, 778
 Helly J. C., Cole S., Frenk C. S., Baugh C. M., Benson A., Lacey C., 2003a, *MNRAS*, 338, 903
 Helly J. C., Cole S., Frenk C. S., Baugh C. M., Benson A., Lacey C., Pearce F. R., 2003b, *MNRAS*, 338, 913
 Jenkins A. et al., 1998, *ApJ*, 499, 20
 Kauffmann G., Colberg J. M., Diaferio A., White S. D. M., 1999, *MNRAS*, 303, 188
 Kauffmann G., White S. D. M., Guiderdoni B., 1993, *MNRAS*, 264, 201
 Lacey C., Cole S., 1993, *MNRAS*, 262, 627

- Lemson G., Kauffmann G., 1999, MNRAS, 302, 111
Mo H. J., Mao S., White S. D. M., 1999, MNRAS, 304, 175
Mo H. J., Yang X., van den Bosch F. C., Jing Y. P., 2004, MNRAS, 349, 205
Postman M., Geller M. J., 1984, ApJ, 281, 95
Seljak U., 2000, MNRAS, 318, 203
Seljak U., Zaldarriaga M., 1996, ApJ, 469, 437
Sheth R. K., 2005, MNRAS, 364, 796
Sheth R. K., Connolly A. J., Skibba R., 2006, MNRAS, submitted (astro-ph/0511773)
Sheth R. K., Mo H. J., Tormen G., 2001, MNRAS, 323, 1
Sheth R. K., Tormen G., 2004, MNRAS, 350, 1385
Somerville R. S., Primack J. R., 1999, MNRAS, 310, 1087
Springel V., 2005, MNRAS, 364, 1105
Springel V. et al., 2005, Nature, 435, 629
Springel V., White S. D. M., Tormen G., Kauffmann G., 2001a, MNRAS, 328, 726
Springel V., Yoshida N., White S. D. M., 2001b, New Astronomy, 6, 79
White S. D. M., Rees M. J., 1978, MNRAS, 183, 341